Applied Catalysis A: General 365 (2009) 48–54

Contents lists available at ScienceDirect

Applied Catalysis A: General

journal homepage: www.elsevier.com/locate/apcata

The influence of metal loading and activation on mesoporous materials supported nickel phosphide hydrotreating catalysts

Tamás I. Korányi [a,*], Alessandro E. Coumans [b], Emiel J.M. Hensen [b], Ryong Ryoo [c], Hei Seung Kim [c], Éva Pfeifer [a], Zsolt Kasztovszky [d]

[a] Chemical Research Center of the Hungarian Academy of Sciences, Budapest, H-1525, Hungary
[b] Schuit Institute of Catalysis, Eindhoven University of Technology, Eindhoven, NL-5600, The Netherlands
[c] National Honor Scientist Program Center for Functional Nanomaterials and Department of Chemistry, KAIST, Daejeon, 305-701, Republic of Korea
[d] Institute of Isotopes of the Hungarian Academy of Sciences, Budapest, H-1525, Hungary

ARTICLE INFO

Article history:
Received 8 April 2009
Received in revised form 10 May 2009
Accepted 26 May 2009
Available online 6 June 2009

Keywords:
Nickel phosphide
SBA-15
KIT-6
Mesoporous MFI
Hydrodesulfurization
Dibenzothiophene
Hydrodenitrogenation
o-Methyl aniline

ABSTRACT

Ordered mesoporous materials (SBA-15 and KIT-6 silica and MFI zeolite) supported nickel phosphide (Ni_xP_y) hydrotreating catalysts were prepared by reduction of oxidic precursors with an initial stoichiometric Ni/P ratio of 2 The metal loading (20 and 30 wt.% Ni_xP_y) and pretreatment conditions (773 K or 873 K reduction temperature, *in situ* sulfidation at 723 K) of the precursors were varied. Temperature programmed reduction, *in situ* XRD, and ^{31}P NMR indicate the formation of metallic nickel then different nickel phosphides (Ni_3P, $Ni_{12}P_5$, then Ni_2P) in this order upon reduction. The changes in the textural properties of the catalysts compared to their parent supports promote the conclusion that a significant part of the Ni_xP_y phases is located inside the mesopores. The catalytic activity (parallel dibenzothiophene hydrodesulfurization and *o*-methyl aniline hydrodenitrogenation) increases strongly with increasing Ni_xP_y loading. The KIT-6 and SBA-15 supported catalysts exhibit higher hydrotreating activities than reference $CoMo/Al_2O_3$ and $Ni_{12}P_5/SiO_2$ catalysts. In contrast, the catalyst based on a mesoporous MFI support had the lowest hydrotreating activity. This activity trend is explained by the propensity of high-surface area mesoporous silica supports to well disperse metal phosphide particles. The active phase composition of the spent catalysts is in the range of $Ni_{2.0-2.6}P_{1.0}S_{0.4-0.7}$. This suggests that bulk Ni_2P with some sulfur in its surface forms the active phase in the mesopores of SBA-15 and KIT-6.

1. Introduction

The continuously decreasing limits for sulfur and nitrogen contents in petroleum-based transformation fuels require the development of improved or novel hydrotreating (hydrodesulfurization (HDS) and hydrodenitrogenation (HDN)) catalysts [1,2]. SBA-15 mesoporous silica-supported nickel phosphides provide better dispersion [3] and higher turnover rates [4] than $NiMo/Al_2O_3$ and Ni_2P/SiO_2 catalysts [5]. Another mesoporous silica applied as support for phosphides is MCM-41 [6–8].

The effects of loading [8,9], pretreatment [6], precursor composition [6,8] and oxide support [5,7,10] were reported on the HDS or HDN properties of nickel phosphides. The nickel phosphide phase present on the support has been shown to depend upon the nickel-to-phosphorus molar ratio of the precursors, the support used, and the TPR conditions employed [11]. Ni_2P has been shown to have superior properties relative to $Ni_{12}P_5$ and Ni_3P for the nickel phosphide phases [11]. This catalytic behavior has been correlated with the structure and surface chemical properties of the phase, and their resistance to sulfur poisoning [12].

SBA-15 is an ordered mesoporous silica composed of two-dimensional hexagonal arrays of channels with typical sizes in the range from 5 to 9 nm [13]. The structure of KIT-6 is the gyroid IPMS structure with cubic *Ia3d* symmetry, structurally similar to smaller-pore MCM-48 silica [14]. MFI zeolites with tunable mesoporosity (mMFI) and strong acidity may bridge the gap between conventional bulk zeolite and amorphous mesoporous aluminosilicates [15]. Typical preparation of nickel phosphides involves the reduction of nickel phosphate catalyst precursors at high temperatures. A disadvantage is the low dispersion of the active phase [16]. Nickel phosphides are resistant to bulk sulfidation and hydrogen sulfide facilitates the reduction process into Ni_2P phases [17].

The aim of this work is to extend our recent study of SBA-15-supported nickel phosphide catalysts [3,4] to examine the influence of metal loading, various activation procedures and the effect of supports on physical, textural and chemical properties and on hydrotreating activities. Ordered mesoporous silicas have a

* Corresponding author. Fax: +36 1 4381143.
E-mail address: koranyi@chemres.hu (T.I. Korányi).

0926-860X/$ – see front matter © 2009 Elsevier B.V. All rights reserved.
doi:10.1016/j.apcata.2009.05.048

high-surface area and are suitable to disperse nickel phosphides. The properties of mesoporous MFI supported nickel phosphides are compared to mesoporous silica supported ones. We modified the conventional high-temperature phosphate reduction method by applying a two-step mild activation procedure in order to improve the dispersion of the resulting nickel phosphide particles. The effect of nickel phosphide loading on the properties and catalytic activities of SBA-15 and KIT-6 supported nickel phosphide catalysts is investigated.

2. Experimental

A series of nickel phosphide containing catalysts were prepared on ordered mesoporous silicas consisted of SBA-15 [13] and KIT-6 [14] and a Na-form of a 5% mesopores-containing MFI (mMFI) with Si/Al = 17 ratio (KJN 175) [15]. SBA-15 has a two-dimensional pore structure and was synthesized from sodium silicate with a triblock copolymer (P123), which was used as a structure directing agent [13]. The mMFI zeolite sample was prepared using 3-[(trimethoxysilyl)propyl]hexadecyl-dimethyl-ammonium chloride (TPHAC), under a slightly modified synthesis condition for ordinary MFI [15].

The supports were impregnated to incipient wetness with a nickel phosphate aqueous solution of the precursors $Ni(NO_3)_2$ and $(NH_4)H_2PO_4$. The initial Ni/P molar ratio of the precursors was adjusted to 2 in the impregnation solution in order to avoid blocking of the mesopores by unreduced phosphate species during the subsequent activation process [4]. For SBA-15 and KIT-6 supports, the loading was adjusted to 20 and 30 wt.% as Ni_2P. The loading was 20 wt.% for mMFI. The SBA-15 supported catalysts are denoted by SBA20 and SBA30, the corresponding KIT-6 supported ones by KIT20 and KIT30, and the mMFI supported catalyst by MFI20. After impregnation the dried precursors were reduced in a hydrogen flow of 200 Ncm^3/min to 623 K at a rate of 3 K/min, then to 873 K at a rate of 1 K/min and kept at this temperature for 1 h. The reduced precursors were cooled to room temperature in nitrogen gas stream for 0.5 h and passivated in a flow of 1 vol% O_2 in N_2 for 1 h at room temperature. A reference silica-supported catalyst containing 20 wt.% $Ni_{12}P_5$ ($Ni_{12}P_5$/SiO2) was prepared in a similar manner. A reference $CoMo/Al_2O_3$ (Shell C444, 9.8 wt.% Mo and 3.4 wt.% Co) was used as received. The dried precursors were characterized by temperature programmed reduction (TPR), during reduction by *in situ* XRD, and the passivated catalysts by nitrogen adsorption and ^{31}P NMR. A novel "mild" two-step activation procedure was explored for some of the dried precursors, which consisted of reduction by hydrogen at 773 K for 2 h in the first step followed by passivation in a flow of 1 vol% O_2 in N_2 for 1 h at room temperature. These "mildly" activated catalysts are denoted as SBA20m, SBA30m, KIT20m, and KIT30m. In the second step the passivated "mild" catalyst was *in situ* sulfided in a flow of 10 vol% H_2S in H_2 gas at a flow rate of 60 Ncm^3/min at 723 K. The heating rate of 6 K/min was followed by an isothermal period at 723 K for 2 h.

During TPR the temperature of the precursor sample was raised from 373 to 940 K by a 1 K/min rate and kept there for 30 min in a 5% H_2/Ar gas stream (flow rate 30 cm^3/min). During *in situ* XRD the precursor sample was reduced in a 70 cm^3/min hydrogen gas stream whilst heating to 723 K by 3 K/min rate followed by further heating to 773, 823, and 873 K by 1 K/min rate. At each of these temperatures the sample was kept isothermal for 1 h during an *in situ* XRD pattern was recorded at the last 50 min. ^{31}P NMR spectra were obtained on a Varian 400-MR spectrometer at 161.9 MHz. The passivated catalyst samples were placed in a 4 mm rotor and spun at 10 kHz. The spectra were acquired using a single 90° P-31 pulse (4 μsec) under high-power proton decoupling conditions using composite pulses. The acquisition time varied between 40 and 25 ms, the recycle time was 1 s and 10000–40000 scans were acquired. The number of active nickel sites was determined by CO chemisorption over the *in situ* reduced passivated catalysts. After rereduction, the catalyst was purged and cooled down to room temperature in helium flow. CO was adsorbed on the samples in 3–4 Torr pressure steps in a 0–30 Torr pressure range. The total and physical CO adsorption isotherms were determined at room temperature and the difference of the two isotherms was regarded as the chemisorbed amount. The ratio of the surface Ni atoms was calculated from the quantity of chemisorbed CO molecules assuming a 1:1 stoichiometry.

An amount of passivated catalyst sieved to a particle size between 125 and 250 μm is diluted with an amount of SiC to achieve isothermal plug-flow conditions in a stainless-steel fixed-bed reactor. After activation, the pressure is increased to 3.0 MPa and the temperature is decreased to 613 K for hydrotreating reactions. The liquid reactant was fed into a hydrogen flow of 500 Ncm^3/min at a rate of 0.1 cm^3/min speed with a high-pressure pump. The composition of the gas phase feed was 70 kPa *n*-decane, 1 kPa (400 ppm) *n*-heptane, 2.5 kPa (800 ppm) *o*-methyl aniline (OMA), and 0.6 kPa (200 ppm) dibenzothiophene (DBT). The reaction products were analyzed by an online gas chromatograph equipped with a CP Sil5-CB capillary column. *n*-Decane and *n*-heptane were used as internal standards for the hydrodesulfurization (HDS) and hydrodenitrogenation (HDN) reactions, respectively. The experiments were carried out for 12–15 h and gas-phase samples were taken every 0.75 h. The main products for the HDS of dibenzothiophene were biphenyl (BP) and cyclohexylbenzene (CHB). For the HDN of OMA, the products were toluene (TOL) and methylcyclohexane (MCH). The DBT HDS and OMA HDN catalytic activities are expressed as pseudo first-order reaction rate constants (k) calculated by Eq. (1) [18].

$$k(\mathrm{mol/kg\,h}) = \frac{-F}{W}\ln(1-X) \quad (1)$$

where F is the molar flow rate of the reactant, W is the mass of the catalyst and X is the reactant conversion.

The nickel, phosphorus and sulfur contents of the spent catalysts following parallel HDS/HDN reactions were determined by prompt-gamma activation analysis (PGAA) [19]. The samples were irradiated in a horizontal cold neutron beam of $1.2 \times 10^8\ cm^{-2}\ s^{-1}$ thermal equivalent flux. The beam size was adjusted to 1 cm × 1 cm, so as to avoid overloading the counting electronics, i.e. not to exceed 1000 counts per second. Since the sample is transparent to neutrons, an average bulk composition of the investigated volume is obtained. The acquisition time for one sample was around 50000 s.

3. Results

3.1. TPR

The H_2-TPR profiles for the five catalyst precursors exhibit two main features. A low temperature reduction profile is observed around 550–650 K and another one in the 750–930 K region (Fig. 1). The profile for the MFI20 catalyst (Fig. 1a) consists of two reduction features close in temperature. This profile differs from those for the KIT-6 and SBA-15 supported catalysts. The first peak can be assigned to the reduction of nickel oxides to metallic nickel [5]. The second broad signal corresponds to the reduction of the phosphate precursor, i.e. to the formation of nickel phosphides [5]. Both peaks shift to higher temperatures when the SBA-15 support is replaced by KIT-6. A shoulder appears around 930 K for the KIT30 catalyst (Fig. 1e), which shows that the reduction is not complete, even at this high temperature.

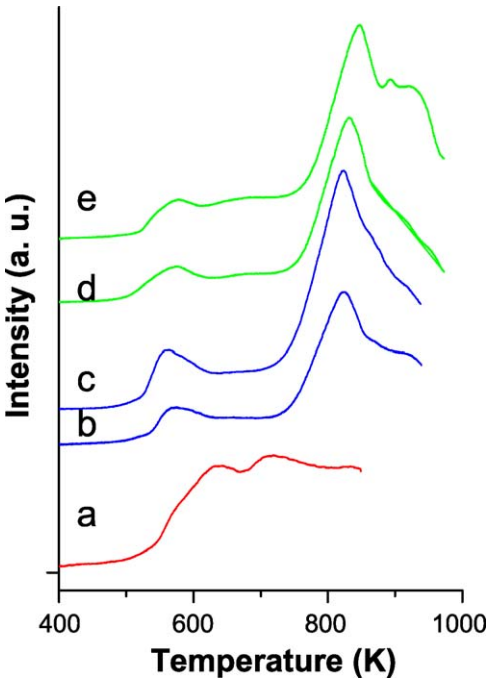

Fig. 1. TPR profiles of MFI20 (a), SBA20 (b), SBA30 (c), KIT20 (d), and KIT30 (e) catalyst precursors. Temperature range from 373 to 940 K, heating rate 1 K/min in a 5% H_2/Ar gas stream (flow rate 30 cm^3/min).

3.2. XRD

The *in situ* XRD patterns demonstrate the presence of metallic nickel and three phosphide phases, i.e. Ni_3P, $Ni_{12}P_5$, and Ni_2P in the catalysts during activation (Figs. 2 and 3, Table 1). Metallic nickel is dominant in most of the catalysts (SBA20 (Fig. 2d), KIT20 (Fig. 2g), $Ni_{12}P_5/SiO_2$ (Fig. 3a) and KIT30 (Fig. 3g) upon reduction at 723 K. Besides Ni, some Ni_3P is evidenced in the patterns of MFI20 (Fig. 2a) and SBA30 (Fig. 3d) at 723 K. The patterns after reduction at 773 K indicate the presence of various phases: a more substantial amount of Ni_3P than Ni appears in MFI20 (Fig. 2b), SBA20 (Fig. 2e) and $Ni_{12}P_5$/SiO2 (Fig. 3b) catalysts than at 723 K,

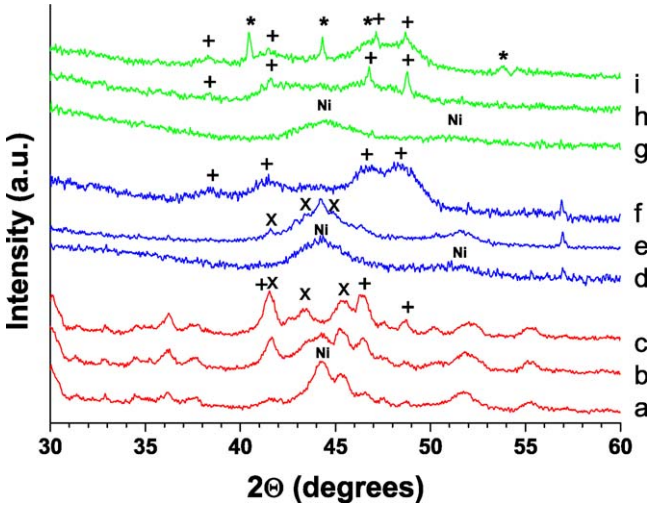

Fig. 2. *In situ* XRD patterns of the catalyst precursors during temperature programmed reduction (3 K/min to 723 K, then 1 K/min to 773 K, each temperature kept for 1 h) in 30 cm^3/min hydrogen stream. Patterns of MFI20 (a–c), SBA20 (d–f), and KIT20 (g–i) catalyst precursors reduced at 723 K (a, d, g), then at 773 K (b, e, h), then at 873 K (c, f, i), respectively. The identified peaks are assigned to metallic nickel (Ni), Ni_3P (X), $Ni_{12}P_5$ (+), and Ni_2P (*) crystalline phases.

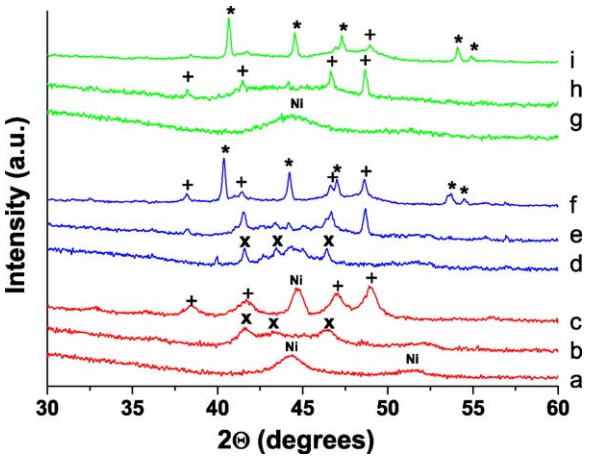

Fig. 3. *In situ* XRD patterns of $Ni_{12}P_5/SiO_2$ (a–c), SBA30 (d–f), and KIT30 (g–i) catalyst precursors during temperature programmed reduction. Conditions are the same as in Fig. 2 caption.

and the characteristic peaks of $Ni_{12}P_5$ are dominant for the KIT20 (Fig. 2h), SBA30 (Fig. 3e) and KIT30 (Fig. 3h) catalysts. A further increase of temperature to 873 K results only in minor changes in the pattern of MFI20 (Fig. 2c), a well dispersed (broad bands) $Ni_{12}P_5$ phase forms for the SBA20 catalyst (Fig. 2f), a mixture of $Ni_{12}P_5$ and Ni_2P forms for the KIT20 (Fig. 2i) and SBA30 (Fig. 3f) catalysts and the characteristic peaks of Ni_2P are dominant in the pattern of the KIT30 (Fig. 3i) catalyst. The pattern for the $Ni_{12}P_5$/SiO2 catalyst is specific: besides the characteristic peaks of $Ni_{12}P_5$ the main peak of metallic nickel reappears at 873 K (Fig. 3c).

3.3. ^{31}P NMR

^{31}P NMR provides additional information on the active phase composition as it is able to detect all ^{31}P nuclei in contrast to XRD. The isotropic phosphide signals (centerbands) are located at 1796 ppm (Ni_3P), 2259 and 1941 ppm ($Ni_{12}P_5$) and 4081 and 1487 ppm (Ni_2P) in the ^{31}P NMR spectra of silica-supported reference catalysts [20]. Ni_3P (Fig. 4a and b), $Ni_{12}P_5$ (Fig. 4c–e and h), and Ni_2P (Fig. 4f, g and i) are observed as the main phosphorus-containing phases in the ^{31}P NMR spectra of MFI20, SBA20m, SBA20, SBA30m, SBA30, KIT30m, KIT20m, KIT20 and KIT30 catalysts, respectively (Table 1). These findings agree with the XRD results for the SBA20m, SBA20, SBA30m, SBA30, KIT30m and KIT30 catalysts (Figs. 2–4, Table 1). This means that the Ni_2P crystallites, which are not yet identifiable by *in situ* XRD in the KIT20m catalyst at 773 K, are already observed by ^{31}P NMR. The reason must be that the crystallites are very small. Paramagnetic phosphates species provide intense signal structures around 0 ppm chemical shift in the ^{31}P NMR spectra of similar catalysts [4]. The spectra of the catalysts do not show evidence for the presence of unreduced phosphate, except for a very weak and noisy phosphate signal in the ^{31}P NMR spectrum of KIT30m catalyst (not shown).

3.4. N_2 porosimetry

The BET surface areas and total pore volumes of the catalysts are much lower than of the parent supports. Moreover, these parameters become lower when the nickel phosphide loading is increased (Table 1). All isotherms are of type IV according to the IUPAC classification [21]. The sorption isotherms of the KIT-6 and SBA-15 supports display relatively narrow type H1 hysteresis loop. The loops of the corresponding catalysts are broader in the desorption branch indicating particles inside the mesoporous

Table 1
Physicochemical data of the various supports and passivated (or spent) phosphide catalysts: BET surface areas (S_{BET}), total pore volumes (V_{pore}), phases identified by XRD and P-containing phases detected by ^{31}P NMR, CO uptakes (n_{CO}) and Ni/P and S/P molar ratios of the spent catalysts.

Support/Catalyst	S_{BET} (m^2/g)	V_{pore} (cm^3/g)	XRD phases	P-containing NMR phases	n_{CO} (μmol/g)	Ni/P molar ratio	S/P molar ratio
SBA-15	720	0.90					
SBA20m	415	0.49	$Ni^{a,b}$ + Ni_3P^b	Ni_3P^b	188		
SBA20	454	0.49	$Ni_{12}P_5^c$	$Ni_{12}P_5^c$	144	2.05	0.70
SBA30	347	0.37	Ni_3P^a + $Ni_{12}P_5^b$ + Ni_2P^c	$Ni_{12}P_5^{b,c}$ + Ni_2P^c	249	2.59	0.56
KIT-6	594	0.79					
KIT20m	496	0.62	Ni^a + $Ni_{12}P_5^b$	Ni_2P^b	171		
KIT20	438	0.57	$Ni_{12}P_5^c$ + Ni_2P^c	Ni_2P^c	125	2.00	0.41
KIT30	362	0.43	Ni^a + $Ni_{12}P_5^b$ + Ni_2P^c	$Ni_{12}P_5^b$ + Ni_2P^c + PO_4^{3-}	223	2.03	0.45
mMFI	433	0.52					
MFI20	389	0.41	Ni_3P^c + $Ni_{12}P_5^c$	Ni_3P^c			

[a] at 723 K.
[b] at 773 K.
[c] at 873 K.

structure and a significant decrease in pore volume with increasing loading (Fig. 5). The shape of the isotherms of the mMFI support and MFI20 catalyst shows the presence of both micro- and mesopores (type H4). As the adsorption takes place dominantly in the low pressure range, the characteristic size of the pores should be in the range of micropores.

The pore size distributions of the supports obtained from the desorption branch of the isotherms using the BJH method are narrower than of the corresponding catalysts (Fig. 6). This difference supports the presence of particles in the mesopores. The mesopore size distributions of the mMFI support and the MFI20 catalyst are quite broad, ranging from 2 to 10 nm. The average mesopore sizes of the KIT-6 and SBA-15 supports and the corresponding catalysts are higher than that of the mMFI support and MFI20 catalyst. The pore size distribution of the phosphide catalysts becomes less homogeneous with increasing loading (Fig. 6), which indicates that some particles are located inside the mesopores partially blocking the cross-sections of the pores. The average diameter of the mesopores of the KIT-6 support and the derived catalysts is around 8 nm. For the SBA-15 support and catalysts the pore size is around 7 nm (Fig. 6).

3.5. CO chemisorption

Surface metal atoms titrated by CO chemisorption provide an estimate for the concentration of active sites in these nickel phosphide catalysts [22]. The CO chemisorption capacities increase with the loading (Table 1). The resulting values are much higher than the highest value (112 μmol/g) reported for Ni_2P/SiO_2 catalysts in literature [7]. Moreover, the dispersion appears to be better for the mildly (573 K) activated SBA20m (188 μmol/g CO) and KIT20m (171 μmol/g CO) catalysts than for the SBA20 (144 μmol/g CO) and KIT20 (125 μmol/g CO) catalysts activated at 873 K (Table 1).

3.6. Parallel DBT HDS and OMA HDN catalytic activities and selectivities

The DBT HDS reaction rate constants of $CoMo/Al_2O_3$ and $Ni_{12}P_5/SiO_2$ reference catalysts are quite stable; they change between 4–5 and 0.5–1 mol/kg h, respectively (Fig. 7). The OMA HDN reaction rate constants of both reference catalysts are below 1 mol/kg h (Fig. 8). The MFI20 catalyst shows very low HDS and HDN activities. Compared to these values the catalysts based on SBA-15 and KIT-6 exhibit good DBT HDS activities (Fig. 7) and excellent catalytic activities in the HDN of OMA (Fig. 8). The HDS activities of KIT20, KIT20m, SBA20 and SBA20m catalysts as well as the HDN activity of SBA20m catalyst increase during the initial 100–300 min of the reactions. The final HDS activity of these catalysts is close to that of

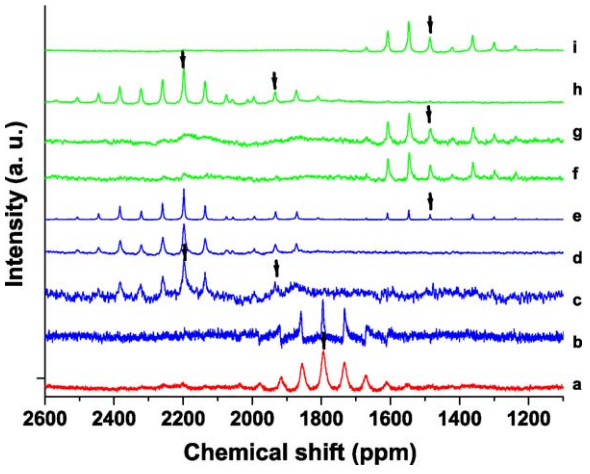

Fig. 4. Nickel phosphide region (2600–1100 ppm) in the ^{31}P NMR spectra of MFI20 (a), SBA20m (b), SBA20 (c), SBA30m (d), SBA30 (e), KIT20m (f), KIT20 (g), KIT30m (h), and KIT30 (i) catalysts. The isotropic signals are indicated by arrows.

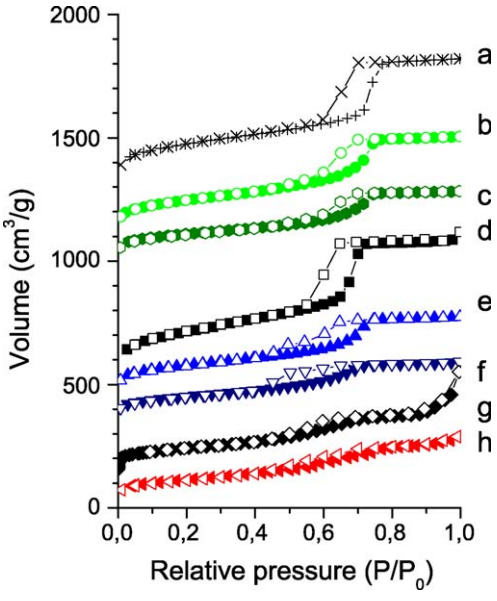

Fig. 5. Nitrogen adsorption–desorption isotherms of the KIT-6 (a), SBA-15 (d) and mMFI (g) supports, and the KIT20 (b), KIT30 (c), SBA20 (e), SBA30 (f) and MFI20 (h) catalysts at 77 K.

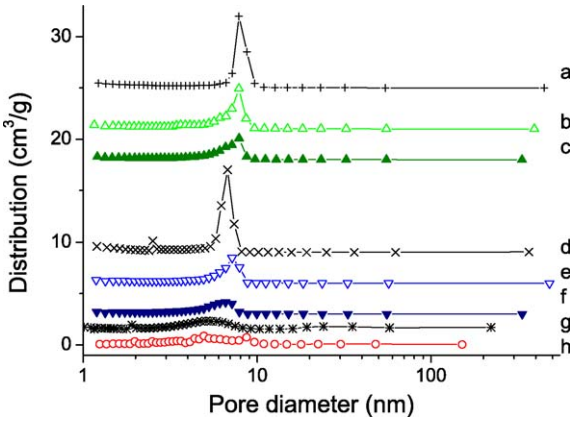

Fig. 6. Pore size distributions of the KIT-6 (a), SBA-15 (d) and mMFI (g) supports, and KIT20 (b), KIT30 (c), SBA20 (e), SBA30 (f) and MFI20 (h) catalysts calculated from the sorption isotherms.

the $CoMo/Al_2O_3$ reference catalyst. Higher loading (SBA30 and KIT30) results in much higher and stable catalytic activities. The DBT HDS activities of SBA30 and KIT30, as well as the OMA HDN activity of SBA30 are outstanding related to either the reference- or the nickel phosphide catalysts with 20 wt.% loadings. No deactivation is observed during the studied 800 min reaction time.

The selectivities for the various catalysts in DBT HDS are very similar at around 92–94% biphenyl selectivities (not shown). An exception is the $CoMo/Al_2O_3$ reference catalyst, for which biphenyl is the only hydrocarbon product (100% selectivity). The biphenyl selectivities increase with time on stream for most catalysts. The biphenyl selectivities of KIT30 and SBA30 catalysts are the lowest. Contrary to the HDS selectivities, the toluene selectivities in HDN (Fig. 9) vary quite strongly among the catalysts. Most of the toluene selectivities do not change with time on stream, except for SBA20m and KIT20m, which show a decrease (Fig. 9). It has been reported that HDS is a structure-insensitive reaction in contrast to HDN [23]. This explains the invariance of the biphenyl selectivity and the strong changes in toluene selectivity. Biphenyl and toluene are the products of C–S and C–N bond breaking reaction pathways, respectively, the other possibility is the hydrogenation route [24]. The selectivity toward biphenyl formation is between 70% and 90%

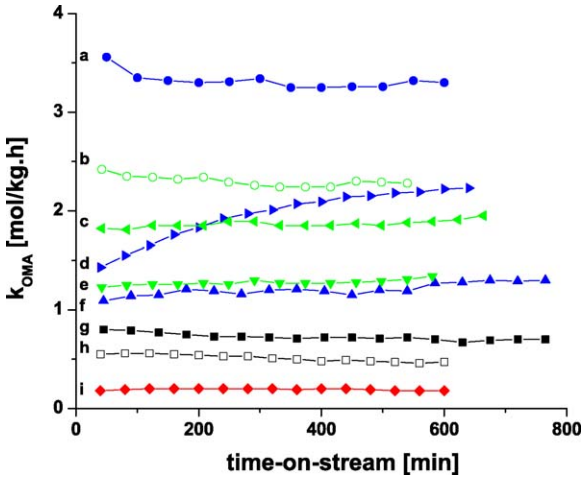

Fig. 8. Pseudo first-order reaction rate constants related to unit catalyst mass for HDN of *o*-methylaniline (OMA) as a function of time on stream over SBA30 (a, ●), KIT30 (b, ○), KIT20m (c, ◀), SBA20m (d, ▶), KIT20 (e, ▼), SBA20 (f, ▲), MFI20 (i, ◆), reference 20 wt.% $Ni_{12}P_5/SiO_2$ (h, □) and commercial $CoMo/Al_2O_3$ (g, ■) catalysts during simultaneous HDS of DBT and HDN of OMA at 613 K and 30 bar.

in the HDS of DBT without N-compounds under similar conditions [25]. The hydrogenation route is strongly suppressed by the inhibiting effect of nitrogen-containing molecules on the surface of the catalysts, as the biphenyl selectivity here is 92–94%. Suppression of hydrogenation is advantageous, because it results in lower hydrogen consumption during hydrotreating.

3.7. Composition of the spent catalysts

The Ni/P and S/P molar ratios of the spent catalysts change between 2.0–2.6 and 0.4–0.7, respectively (Table 1). The bulk composition, $Ni_{2.0-2.6}P_{1.0}S_{0.4-0.7}$, suggests the presence of a nickel phosphosulfide active phase. We earlier suggested a $Ni_{2.7}P_{1.0}S_{0.24}$ surface composition of the active phase for a sulfided SBA20 catalyst [4]. It is indeed reasonable to assume that some *in situ* sulfidation of the surface nickel phosphide phase takes place to a nickel phosphosulfide, as originally proposed by us [17] and later by others [9,11,23,26].

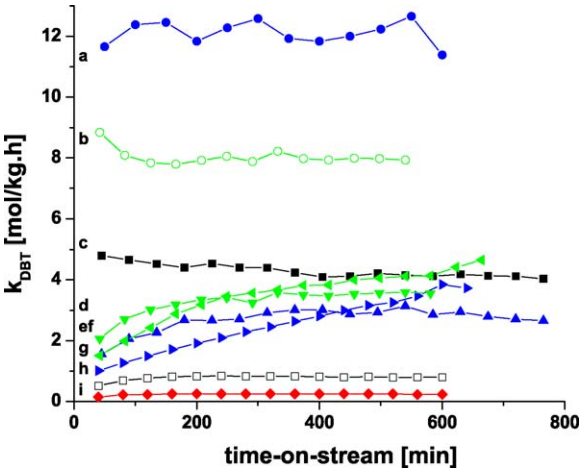

Fig. 7. Pseudo first-order reaction rate constants related to unit catalyst mass for HDS of dibenzothiophene (DBT) as a function of time on stream over SBA30 (a, ●), KIT30 (b, ○), KIT20 (d, ▼), KIT20m (e, ◀), SBA20 (f, ▲), SBA20m (g, ▶), MFI20 (i, ◆), reference 20 wt.% $Ni_{12}P_5/SiO_2$ (h, □) and commercial $CoMo/Al_2O_3$ (c, ■) catalysts during simultaneous HDS of DBT and HDN of OMA at 613 K and 30 bar.

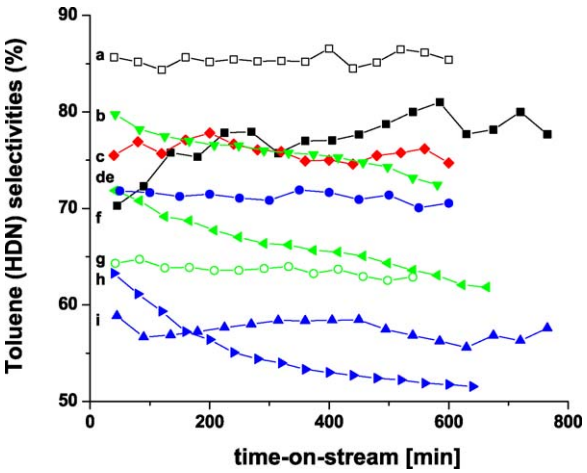

Fig. 9. Toluene product selectivities of OMA HDN as a function of time on stream over KIT20 (b, ▼), MFI20 (c, ◆), SBA30 (d, ●), KIT20m (e, ◀), KIT30 (g, ○), SBA20m (h, ▶), SBA20 (i, ▲), reference 20 wt.% $Ni_{12}P_5/SiO_2$ (a, □) and commercial $CoMo/Al_2O_3$ (f, ■) catalysts during simultaneous HDS of DBT and HDN of OMA at 613 K and 30 bar.

4. Discussion

4.1. Characterization

Nickel phosphides are formed in two steps during the reduction of the oxidic precursors at high initial Ni/P ratio: the first step is the reduction of Ni^{2+} to metallic nickel followed by the formation of nickel phosphide(s) from reduction of the phosphate [5]. Due to the very broad TPR signals (Fig. 1), the details of these reduction processes cannot be studied. *In situ* XRD reveals the formation of various nickel phosphides during the reduction process. Metallic nickel is formed first followed by the formation of Ni_3P. This transformation can be clearly observed from the XRD patterns for the MFI20, SBA20 and $Ni_{12}P_5/SiO_2$ catalysts going from 723 to 773 K (Figs. 2 and 3). The presence of Ni_3P phase is dominant only in the pattern of SBA30 at 723 K (Fig. 3d), which means that the reduction of this precursor is the easiest process at this temperature. At 773 K $Ni_{12}P_5$ becomes the dominant phase in the patterns of KIT20, KIT30 and SBA30, and at 873 K Ni_2P appears in the patterns of same three precursors. The ^{31}P NMR spectra provide further insight into the reduction processes. The TPR profiles (Fig. 1) explain the appearance of traces of phosphates in the ^{31}P NMR spectra as the reducibility of KIT30 is the most difficult among the four samples at 773 K. The formation of Ni_2P from $Ni_{12}P_5$ can already be deduced at 773 K for the KIT20m and at 873 K for the SBA30 catalyst (Fig. 4f and e). The ^{31}P NMR spectra clearly reveal that Ni_3P is the dominant nickel phosphide phase for the MFI20 catalyst at 873 K. Accordingly, the formation of active phases follows the order Ni, Ni_3P, $Ni_{12}P_5$ and Ni_2P with increasing the temperature of reduction.

Evidence for the occurrence of phosphide-oxide support interactions was earlier found from time-resolved XRD measurements [27]. This interaction enhances the stability of intermediate phosphide phases which do not occur in unsupported nickel phosphides. The reported order is in agreement with the present phosphate – Ni – Ni_3P – $Ni_{12}P_5$ – Ni_2P order of reduction during the activation process. According to Rodriguez et al. [27], $Ni_{12}P_5$ is the reactive intermediate to Ni_2P and more phosphorus is needed to form Ni_2P. It is generally believed, that an excess of phosphorus in the precursors is necessary for the preparation of silica-supported Ni_2P [9,20,23]. A drawback of this approach for ordered mesoporous silicas is that the narrow mesopores can be blocked by unreduced phosphate species, in case an excess of phosphorus is introduced during the preparation [4]. Therefore, we employed a stoichiometric amount of phosphorus (Ni/P ratio of 2) in this work. The gradually decreasing surface areas and pore volumes, the broader hysteresis loops and less homogeneous pore size distributions of the prereduced (activated) catalysts with increasing loading show that a significant part of the nickel phosphide phase is located inside the mesopores. The shape of the isotherms does not evidence extensive pore blocking.

Both the loading of the active phase and the support influenced the reduction process and the formation of nickel phosphide(s). The reduction of KIT30 catalyst was not complete even at 930 K (Fig. 1). The MFI20 catalyst was reduced until Ni_3P phase only, the SBA20 catalyst for $Ni_{12}P_5$ and the KIT20 catalyst to Ni_2P at 873 K (Figs. 2 and 4).

4.2. Catalytic activity

The pseudo first-order reaction rate constants (k values in Eq. (1)) can be corrected for differences in the dispersion of surface nickel atoms using active site densities determined by CO chemisorption [1,22]. The surface state of nickel phosphide catalysts is changing during the hydrotreating reaction as partial sulfidation of the nickel surface is carried out [1,4]. Therefore, initial conversions (X) and initial pseudo first-order reaction rate constants related for unit catalyst mass (k_{mass} (mol/kg h)) and for unit active site (k_{site} in (h^{-1}) and (s^{-1}) dimensions) are presented in Table 2 for comparison purposes.

The CO uptakes (n_{CO} in Table 1) and intrinsic reaction rate constants (k_{site} (s^{-1}) in Table 2) are comparable with literature data. The latter rate constants are sometimes incorrectly named turnover numbers (TONs) in the literature [5]. The highest CO uptakes published for fresh Ni_2P/SiO_2 and Ni_2P/MCM-41 catalysts are 112 and 139 μmol/g, respectively [7], which are similar or smaller (Table 1) than those for SBA-15 and KIT-6 supported nickel phosphide catalysts. Accordingly, the high hydrotreating activity of the SBA-15 and KIT-6 mesoporous material supported catalysts can be ascribed to its high specific surface areas and the improved dispersion of the phosphide active phase. TONs were 0.0015 [5] and 0.0030 s^{-1} [26] for DBT HDS, and 0.0006 s^{-1} [5] for quinoline HDN over Ni_2P/SiO_2 catalysts. These TON values were measured in single DBT HDS [26] and parallel DBT HDS and quinoline HDN [5] reactions. The twofold decrease in the TON of DBT HDS is the consequence of adsorption of nitrogen containing molecules on the catalyst surface [25]. These molecules affect the relative reactivities and reaction pathways in hydrotreating reactions [28]. TONs for DBT HDS published in the literature [5,26] are similar for the least active (SBA20m, KIT20m and SBA20) catalysts, but much smaller than those for SBA30 and KIT30 catalysts. The TON for quinoline is not comparable with the TON for OMA, but TONs for OMA are not found in the literature. Accordingly the DBT HDS activity of SBA30 and KIT30 catalysts is about one order of magnitude higher than those of the most active hydrotreating catalysts published in the literature.

Table 2
Initial conversions (X) and initial pseudo first-order reaction rate constants related for unit catalyst mass (k_{mass} (mol/kg h)) and for one active site (k_{site} (h^{-1}) and (s^{-1})) calculated from CO adsorption over various catalysts for DBT HDS (top) and OMA HDN (bottom).

HDS/HDN	CoMo[a]	Ni_2P[b]	SBA10[c]	SBA20m	SBA20	SBA30	KIT20m	KIT20	KIT30	MFI20
X (%)	86.1	19.2	9.0	34.1	47.4	91.1	46.1	57.3	97.4	6.1
k_{mass}[d]	4.8	0.5	0.2	1.0	1.6	11.7	1.5	2.1	8.8	0.2
k_{site}[e] (h^{-1})				5.4	10.8	46.8	8.8	16.6	39.6	
k_{site}[f] (s^{-1})				0.0015	0.0030	0.0130	0.0024	0.0046	0.0110	
X (%)	7.4	5.2	3.8	13.0	10.0	16.3	16.4	11.5	21.4	1.7
k_{mass}[d]	0.8	0.5	0.4	1.4	1.1	3.6	1.8	1.2	2.4	0.2
k_{site}[e] (h^{-1})				7.6	7.6	14.3	10.6	9.8	10.8	
k_{site}[f] (s^{-1})				0.0021	0.0021	0.0040	0.0030	0.0027	0.0030	

[a] $CoMo/Al_2O_3$.
[b] Ni_2P/SiO_2.
[c] SBA-15 supported catalyst with 10 wt.% nickel phosphide loading reduced at 873 K.
[d] calculated by Eq. (1).
[e] k_{site} (h^{-1}) = k_{mass} (mol/kg h)/n_{CO}.
[f] k_{site} (s^{-1}) = k (h^{-1})/3600.

In order to reach high hydrotreating activities the effect of various pretreatments, in other words the activation process, seems to be less important than the effect of the active phase loading. There is approximately a 60-fold increase of the initial DBT HDS activity and a one order of magnitude increase of the initial OMA HDN going from SBA10 through SBA20 to SBA30 catalysts (k_{mass} in Table 2). One possible explanation for this finding is that the activation of SBA20 and KIT20 catalysts is not complete upon pretreatment and continues during the catalytic reaction. There are, indeed, fourfold and threefold increases in k_{HDS} activities for SBA20m and KIT20m, respectively, during the catalytic reaction (Fig. 7). Both (biphenyl and toluene) product selectivity of the two catalysts changes parallel during the catalytic reaction (Fig. 9). The lower reduction degree of SBA20m (Ni_3P) compared to KIT20m ($Ni_{12}P_5$) is reflected in the increasing k_{OMA} activity of the former and the stable k_{OMA} values of the latter during the reaction (Fig. 8). The activities of KIT30 and SBA30 catalysts are not increasing during the catalytic reaction contrary to the catalysts with 20 wt.% loadings, because the reduction degrees of the former catalysts are closer to the Ni_2P state than that of the latter ones at 873 K. It is clearly seen in the ^{31}P NMR spectra (Fig. 4).

The further activation of nickel phosphide catalysts during the catalytic reaction poses the question about the real nature of the active phase. Ni_2P [10,17], a surface phosphosulfide with unknown stoichiometry [23], and surface Ni_3PS from DFT calculations [29] are the possible nominees. The compositions of spent SBA20, SBA30, KIT20 and KIT30 catalysts were determined by the PGAA method. Accordingly, the active phase composition of the most active SBA30 catalyst is $Ni_{2.6}P_{1.0}S_{0.6}$, while that of the other catalysts is $Ni_{2.0}P_{1.0}S_{0.4–0.7}$. We suggest that the active phase is made up of bulk Ni_2P with some sulfur on its surface.

An important question is the role of support in these reactions. Only minor differences were found between the SBA-15 and KIT-6 supported catalysts, if the pretreatment was carried out in the same way. The activity of the MFI20 catalyst was the lowest. The main difference between the SBA-15 and KIT-6 supports is the two-dimensional structure of the former and the three-dimensional structure of the latter. This reflects in the somewhat lower reducibility of the SBA20 than that of the KIT20 catalyst (Table 1, Figs. 1–4). The reducibility of SBA30 catalyst is higher than that of the KIT30 catalyst at 723 K temperature only. A reversed order is observed at 873 K: only Ni_2P is detected in KIT30, while the mixture of $Ni_{12}P_5$ and Ni_2P in the SBA30 catalyst according to the XRD patterns and the NMR spectra. In other words the SBA-15-supported catalysts contain the $Ni_{12}P_5$ active state phase in a longer temperature range than the KIT-6-supported catalysts. This can be explained by the difference in their pore structures only. Another difference is the surprisingly uniform initial k_{site} activities of KIT-6 supported catalysts in OMA HDN. This result can be explained again with the easier reducibility of KIT20 compared to SBA20 catalysts due to the three-dimensional structure of the former and the two-dimensional structure of the latter. The lowest activity of the MFI20 catalyst is most likely the consequence of relatively low mesopore volume of this material (Fig. 5). Moreover, the presence of acidity in the mMFI support is undesirable for phosphide catalysts [30]. From TPR (Fig. 1), it is also clear that the reducibility of this material is the lowest. The XRD (Fig. 2) and ^{31}P NMR (Fig. 4) data confirm this. The dominant phases of nickel phosphides are different on the different supports: they are Ni_3P for the mMFI-, $Ni_{12}P_5$ for the SBA-15- and Ni_2P for the KIT-6 supports at 873 K (Table 1, Figs. 2 and 4).

5. Conclusions

The formation of nickel phosphide was studied on mesoporous-silica (SBA-15 and KIT-6) and -zeolite (mMFI) supported catalysts by *in situ* XRD during temperature programmed reduction and by ^{31}P NMR. Active phases formed in the order Ni, Ni_3P, $Ni_{12}P_5$ and Ni_2P with increasing the temperature of reduction. Using an initial stoichiometric Ni/P ratio of 2 leads to the formation of first nickel and then nickel-rich phosphides like $Ni_{12}P_5$ known to be poorly HDS active. Both the loading of the active phase and the support influenced the reduction process, the formation of nickel phosphide(s). The reduction of the mMFI supported catalyst was more difficult than the others. The support significantly affected the formation of nickel phosphides: Ni_3P, $Ni_{12}P_5$ and Ni_2P were the dominant phases in the MFI20, SBA20 and KIT20 catalysts at 873 K, respectively.

The formation of the active phase(s) continued even during the hydrotreating reaction. Nickel phosphosulfides with undefined composition are suggested as the real active phases. The SBA-15 and KIT-6 supported nickel phosphide catalysts with 30 wt.% loading provide prominent intrinsic parallel DBT HDS and OMA HDN hydrotreating activities.

Acknowledgments

T.I.K. acknowledges F.N.R.S. (Belgium) the financial support. The authors are indebted to Prof. J. B.Nagy (Namur, Belgium) for making available NMR facilities.

References

[1] S.T. Oyama, J. Catal. 216 (2003) 343.
[2] J. Hancsók, G. Nagy, Gy. Pölczmann, Á. Beck, D. Kalló, Stud. Surf. Sci. Catal. 174B (2008) 1159.
[3] T.I. Korányi, Z. Vít, J. B.Nagy, Catal. Today 130 (2008) 80.
[4] T.I. Korányi, Z. Vít, D.G. Poduval, R. Ryoo, H.S. Kim, E.J.M. Hensen, J. Catal. 253 (2008) 119.
[5] X. Wang, P. Clark, S.T. Oyama, J. Catal. 208 (2002) 321.
[6] A. Wang, L. Ruan, Y. Teng, X. Li, M. Lu, J. Ren, Y. Wang, Y. Hu, J. Catal. 229 (2005) 314.
[7] S.T. Oyama, Y.-K. Lee, J. Catal. 258 (2008) 393.
[8] J.A. Cecilia, A. Infantes-Molina, E. Rodríguez-Castellón, A. Jiménez-López, J. Catal. 263 (2009) 4.
[9] S.J. Sawhill, D.C. Phillips, M.E. Bussell, J. Catal. 215 (2003) 208.
[10] W.R.A.M. Robinson, J.N.M. van Gestel, T.I. Korányi, S. Eijsbout, A.M. van der Kraan, J.A.R. van Veen, V.H.J. de Beer, J. Catal. 161 (1996) 539.
[11] S.J. Sawhill, K.A. Layman, D.R. Van Wyk, M.H. Engelhard, C. Wang, M.E. Bussell, J. Catal. 231 (2005) 300.
[12] V. Zuzaniuk, R. Prins, J. Catal. 219 (1993) 85.
[13] M. Choi, W. Heo, F. Kleitz, R. Ryoo, Chem. Commun. (2003) 1340.
[14] T.-W. Kim, F. Kleitz, B. Paul, R. Ryoo, J. Am. Chem. Soc. 127 (2005) 7601.
[15] M. Choi, H.S. Cho, R. Srivastava, C. Venkatesan, D.-H. Choi, R. Ryoo, Nat. Mater. 5 (2006) 718.
[16] S. Yang, C. Liang, R. Prins, J. Catal. 237 (2006) 118.
[17] T.I. Korányi, Appl. Catal. A 239 (2003) 253.
[18] V.H.J. de Beer, T.H.M. van Sint Fiet, J.F. Engelen, A.C. van Haandel, M.W.J. Wolfs, C.H. Amberg, G.C.A. Schuit, J. Catal. 27 (1972) 357.
[19] Zs. Révay, T. Belgya, Zs. Kasztovszky, J.L. Weil, G.L. Molnár, NIMB 213 (2004) 385.
[20] C. Stinner, Z. Tang, M. Haouas, Th. Weber, R. Prins, J. Catal. 208 (2002) 456.
[21] K.S.W. Sing, D.H. Everett, R.A.W. Haul, L. Moscou, R.A. Pierotti, J. Rouquerol, T. Siemieniewska, Pure Appl. Chem. 57 (1985) 603.
[22] S.T. Oyama, X. Wang, Y.-K. Lee, K. Bando, F. Requejo, J. Catal. 210 (2002) 207.
[23] S.T. Oyama, X. Wang, Y.-K. Lee, W.-J. Chun, J. Catal. 221 (2004) 263.
[24] M. Houalla, N.K. Nag, A.V. Sapre, D.H. Broderick, B.C. Gates, AICHE J. 24 (1978) 1015.
[25] M. Egorova, R. Prins, J. Catal. 221 (2004) 11.
[26] F. Sun, W. Wu, Z. Wu, J. Guo, Z. Wei, Y. Yang, Z. Jiang, F. Tian, C. Li, J. Catal. 228 (2004) 298.
[27] J.A. Rodriguez, J.-Y. Kim, J.C. Hanson, S.J. Sawhill, M.E. Bussell, J. Phys. Chem. B 107 (2003) 6276.
[28] R. Prins, Adv. Catal. 46 (2001) 399.
[29] A.E. Nelson, M. Sun, A.S.M. Junaid, J. Catal. 241 (2006) 180.
[30] T.I. Korányi, É. Pfeifer, J. Mihály, K. Föttinger, J. Phys. Chem. A 112 (2008) 5126.